We are IntechOpen, the world's leading publisher of Open Access books Built by scientists, for scientists

6,900
Open access books available

186,000
International authors and editors

200M
Downloads

Our authors are among the

154
Countries delivered to

TOP 1%
most cited scientists

12.2%
Contributors from top 500 universities

WEB OF SCIENCE™

Selection of our books indexed in the Book Citation Index
in Web of Science™ Core Collection (BKCI)

Interested in publishing with us?
Contact book.department@intechopen.com

4

IR Barrier Data Integration for Obstacle Detection

J. Jesús García, Jesús Ureña, Manuel Mazo and Álvaro Hernández
University of Alcalá
Spain

1. Introduction

The great development of the railway as a mean of transport makes necessary more and more reliable the required safety systems. Among these systems, those called detectors of the fall of objects can be remarked, mainly demanded in the high-speed lines, to detect the existence of objects on the track supposing a risk (larger than 50x50x05cm) for the railway circulation in some specific areas such as tunnels and overpasses (GIF, 2001). This type of systems is based on different sensory elements; in (GIF, 2001) it is proposed one based on infrared (IR) barriers, where links are established between emitters and receivers. The detection of objects is carried out by the interruption of these links. But this system can be lacking in reliability, mainly due to outdoor problems related to IR sensors.

In this chapter, it is proposed a new system, based on an IR barrier as well, but including an algorithm to validate the existence of obstacles, increasing the reliability of the detection system. First of all, to be able to discriminate the different emissions in a receiver, it is necessary to encode them. The detection of the emissions is carried out by correlation (Tseng, Shu-Ming & Bell, 2000), where a detection threshold is defined to evaluate if the link is active or not. Because the detection of objects is based on the radiation lack at the receivers, this circumstance does not always imply the existence of a dangerous object for the railway, generating false alarms. The adverse climatology also gives the degradation of the optical channel, so the radiation lack in these circumstances can be confused with the existence of objects.

Furthermore, in some cases small objects can interrupt the links (falling leaves, small animals, etc.), or even a wrong operation of a sensor can be confused with the existence of an object, generating false alarms. To avoid these situations, in this work different procedures are proposed to conclude if there are dangerous objects in the scanned area.

Therefore, the starting point is the information provided by the IR receivers: the result of the correlation, and a threshold output indicating if the link is active. The information about the state of the links (*on* or *off*) is combined by means of the Dempster-Shafer evidential theory (Klein, 2004) taking into account the channel degradation and the spatial diversity of the sensory system structure, so a certainty value can be obtained about the existence objects larger than 50x50x50 cm.

Regarding this problem, the following aspects will be analyzed in this chapter: description of the structure of the sensory system; main factors of infrared channel degradation; a brief explanation about the proposed encoding scheme and the detection of the emissions; sensor

data fusion to obtain the existence certainty of dangerous obstacles based on Dempster Shafer's rule; real tests; and finally, the most relevant conclusions.

2. Description of the sensory system

2.1 Sensory system

For the application described in the previous section, either infrared or laser emitters could be used. Irrespective of the sensor type chosen, all the details that will be discussed below can be applied to both types. The choice of the system may depend on financial considerations. In this work, the results shown have been obtained using infrared emitters, mainly because this kind of sensor was required by Spanish Railway Regulations (GIF, 2001).

Infrared barriers usually consist of emitter-receiver pairs, each placed on opposing sides of the line, so it is only possible to detect the presence of an obstacle, but not its exact position. In order to detect obstacles on the railway, and distinguish at least vital areas (on the track) from the non-vital areas (to the side of the track), a special structure has been designed. In this case, every emission is detected by several receivers, providing different optical links among the emitters and the receivers as is shown in Figure 1.
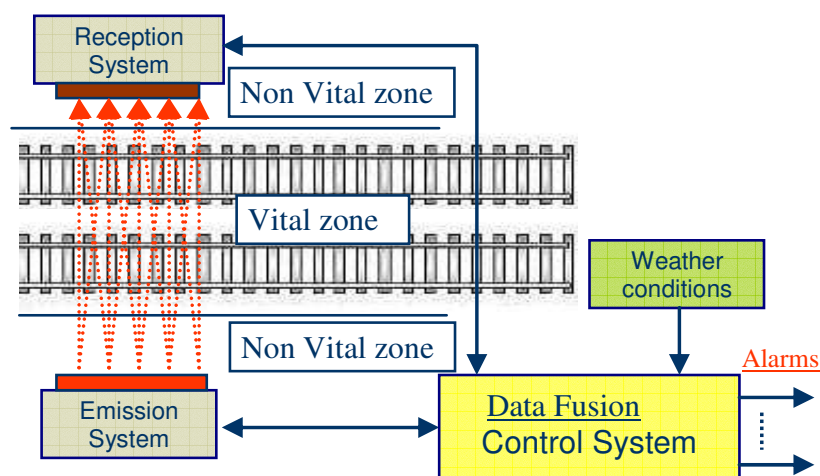

Fig. 1. Detection system placed on a section of track.

The distance between emitting sensors is 25 cm, in order to detect 50x50x50cm obstacles successfully (the size is determined by railway regulations) (GIF, 2001). The configured distance between emitters and receivers is 14 meters on a high-speed line. Basically, the method of obstacle detection, and its location on the railway, is based on the lack of reception by detectors. According to (GIF, 2001) the time scan of the system is 500 ms, and if an obstacle is inside the detection area more than 3 seconds, an alarm should be generated. For a more detailed study about the sensory system see (García et al., 2004). Figure 2 shows the scheme of the infrared barrier, and how when there a minimum dimension object, at least two links are interrupted.

2.2 Geometric distribution of the sensors

Taking into account the infrared emitter beam angle ($\approx\pm2°$), if the range is 14 meters, every emission reaches five receivers, as Figure 3 shows; and reciprocally, every receiver has to detect five emissions.
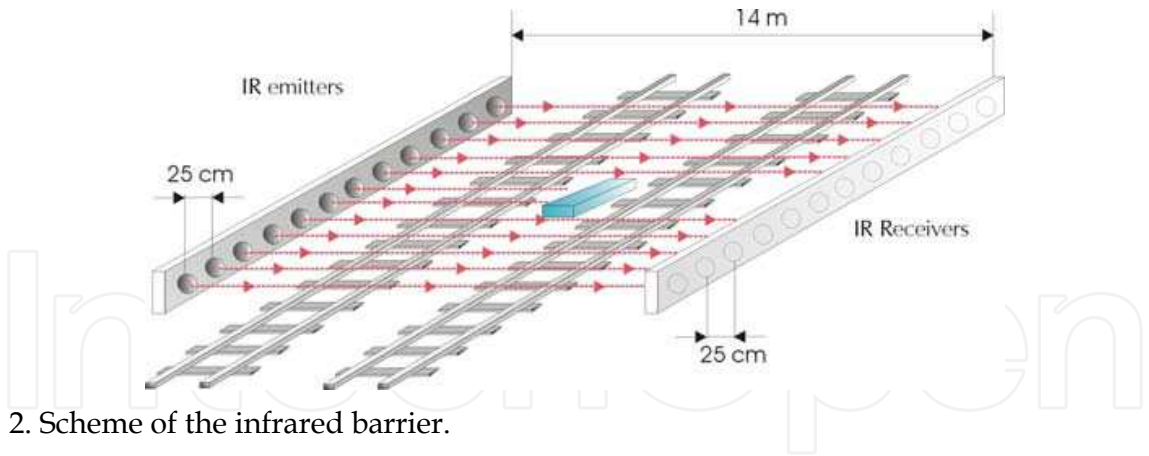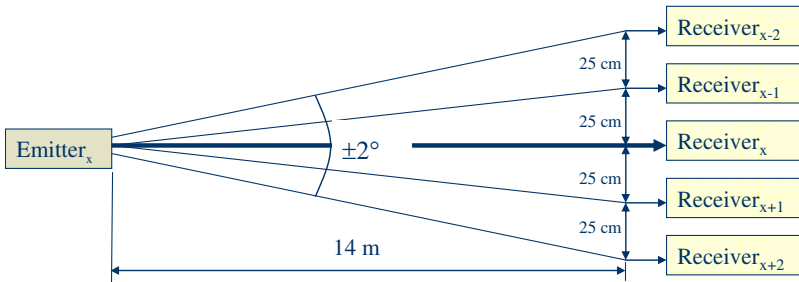
Fig. 2. Scheme of the infrared barrier.

Fig. 3. Emitter-receivers links.

Figure 4 shows the distribution of sensors at a 2.25m segment of the barrier, displaying the five links that every emitter provides. Regarding the sensors distribution, and as it will be explained in Section 4, it is necessary to use five different codes to distinguish every emission in a receiver.
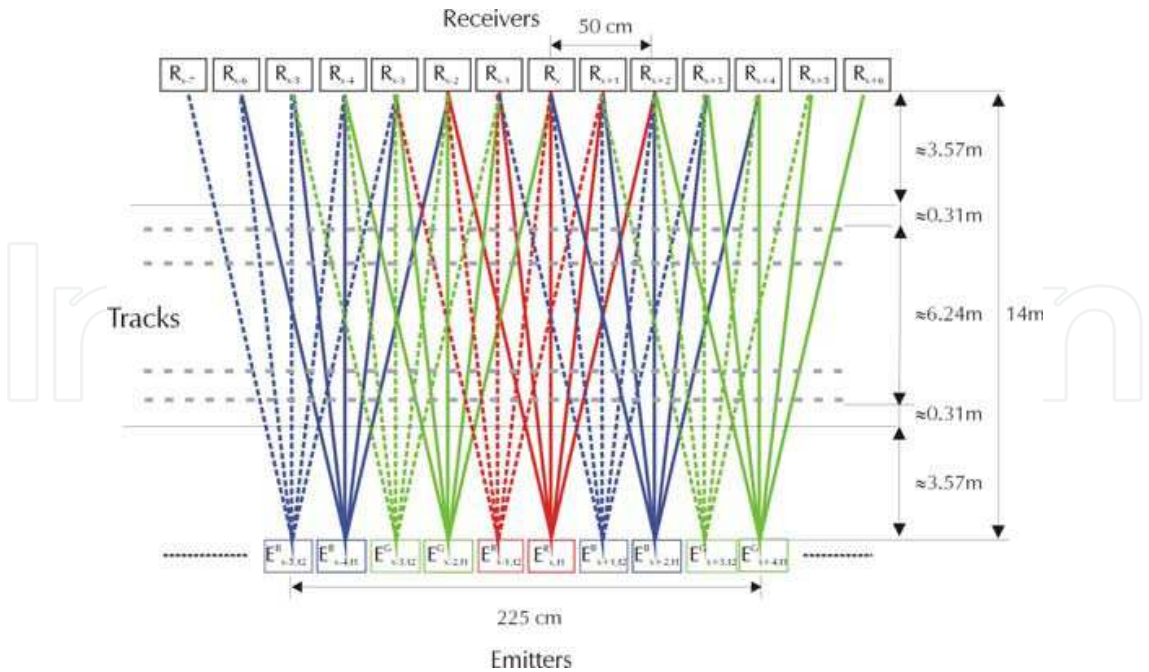

Fig. 4. Distribution of emitters and receivers.

There are some improvements with the structure shown in Figure 4. On the one hand, if there is a minimum dimension obstacle in the supervised area, at least ten links are

interrupted. In (GIF, 2001, 2004) only two interrupted links are required to detect the obstacle. On the other hand, due to the fact that detection is based on link interruption, if a sensor is not working, it can be mistaken for the detection of one obstacle. The number of interrupted links allows the system to distinguish the presence of an obstacle from an out of order sensor, being of particular advantage to those carrying out maintenance tasks. Finally, the obstacles can be located with this structure in two main zones: on the tracks or outside of the tracks.

3. Infrared channel degradation

The outdoor infrared emission suffers from diverse losses, which can produce a wrong detection in the receiver. If the receiver does not detect one emission during a predefined time, an alarm will be generated, informing that there is an obstacle. But if the obstacle does not exist, the alarm is actually false. As far as possible, it is necessary to avoid the false alarms generation. So, it is very important to consider those circumstances that can produce infrared channel degradation.

In these outdoor optical systems there are some phenomena that can provide false alarms, mainly the weather condition and the solar radiation. There are other reasons, as propagation losses or wrong alignment among emitters and receivers. Assuming that the last ones have been already considered in the link design, only the two first are described below:

Atmospheric attenuation. Snow, fog and rain are considered. Although there are numerous studies about the losses due to the meteorology, the expression (1) is used to quantify atmospheric attenuation (Yokota et al., 2002).

$$L_{atm}(dB) = \frac{13}{V} \cdot R \qquad (1)$$

where V is the visibility in kilometres and R the link range in kilometres. The technical definition of visibility or visual range is the distance that light decreases to 2% of the original power, or qualitatively, visibility is the distance at which it is just possible to distinguish a dark object against the horizon (Kim et al., 2000). Table 1 shows the relation between weather condition and the visibility.

Visibility V	Weather condition
V>50km	Very clear
6km<V<50km	Clear
1km<V<6km	Haze /snow /light rain
0.5km<V<1km	Light fog /snow / heavy rain
V<0.5km	Thick fog

Table 1. Relation between visibility and weather condition.

Taking into account (1), in a 14 meters link (the distance among emitters and receivers in the obstacle detection system), atmospheric attenuation θ_k in the time instant k is

$$\theta_k = 10^{-\frac{18.5}{V_k}} \qquad (2)$$

where V_k is the value of the visibility in the instant *k*. Some authors use a different expression (Kim et al., 1998) for atmospheric losses, taking into account the wavelength of the emission and the size distribution of the scattering particles, related to the visibility. Nevertheless, the obtained results with both expressions are similar.

Solar interference. As the photodiode wavelength (850nm) is inside the solar spectrum, natural background light can potentially interfere with signal reception. In some circumstances, direct sunlight may cause link outages for periods of several minutes when the sun is within the receiver's field of view (Bloom et al., 2003). However, the times, when the receiver is most susceptible to the effects of direct solar radiation (either at dawn or at dusk), can be easily estimated. There are some solutions to mitigate this problem, like proper orientation or use of a narrow-bandwidth light filters, but it is almost impossible to avoid them completely. It is important to remember that interference by reflected sunlight is possible as well. The solar effect in the IR barrier is the photodiode saturation.

4. Encoding scheme and detection of the emissions

As has been previously described, a multi-mode operation is carried out in the barrier (simultaneous multi-emission and multi-reception). Therefore it is necessary to encode every emission in order to avoid interferences among the different emissions and to discriminate them at the receiving block.

Due to the fact that the obstacle detection is based on a lack of signal in the receiver, sometimes it can be produced by atmospheric attenuation. Furthermore, solar interference is a high source of noise that can make impossible to distinguish the emissions in the reception system, producing false alarms.

For the mentioned reasons, it is necessary to choose an encoding scheme that permits the multi-mode operation under low signal-to-noise ratios. Trying to answer these requirements, mutually orthogonal complementary sets of sequences have been used (Tseng, Shu-Ming & Bell, 2000)(Chow, 2003)(De Marziani, 2007) for encoding the emissions. More details about the codification scheme and the adaptation to the infrared sensor can be found in (Diaz et al., 2007).

In Figure 4, every emitter uses a different code (shown by different colour in the diagram). The detection of the different emissions is carried out by means of a correlation process, where the output of every receiver provides five measurements, corresponding to the correlation values obtained for every link, as Figure 5 shows. Due to the fact that the emitters transmit periodically, the correlation output obtained for every link is a periodic signal as shows (3).

$$y_k^{(j,x)} = G \cdot \theta_k \cdot \sigma_j \cdot \sum_{i=0}^{i=\infty} \delta[k - i \cdot T] + \phi_{\eta,k} \tag{3}$$

In (3), *G* is the process gain, according to the encoding scheme (Diaz et al., 2007); *T* is the emission period (around 100ms); θ_k represents atmospheric attenuation described in (2); σ_j is the lateral attenuation (it depends on the sensor emission pattern (Diaz et al., 2007)); $\phi_{n,k}$ is the noise component after the correlation; *x* is the position of the receiver in the barrier and $j \in \{1, 2, 3, 4, 5\}$ represents every link established in a receiver, as shown in Figure 5. The index *k* represents the time instant when data are captured.
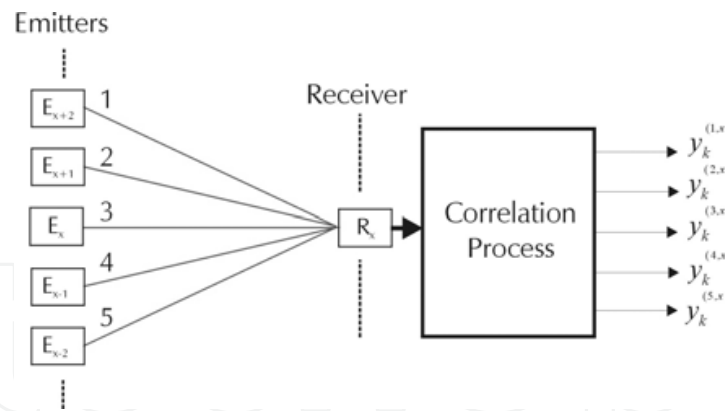
Fig. 5. Block diagram of the detection process.

According to Figure 5, the output of every receiver can be represented as a vector $\mathbf{y}_k^{(x}$ of five measurements, as (4) shows

$$\mathbf{y}_k^{(x} = \begin{bmatrix} y_k^{(1,x} & y_k^{(2,x} & y_k^{(3,x} & y_k^{(4,x} & y_k^{(5,x} \end{bmatrix}^T \tag{4}$$

where x is the position of the receiver in the barrier; and k represents the time instant. Every component of vector $\mathbf{y}_k^{(x}$ is represented in (3). Figure 6 shows the multi-detection carried out in an IR receiver in absence of obstacles. The amplitude differences depend on the lateral deviations between emitters and receiver (see Figures 3 and 4), so the maximum correlation output is provided by the emitter placed in the axial axis.

In (5), the matrix $\mathbf{Y}_k$ contains the correlation output of all the links in the IR barrier. Every column of matrix $\mathbf{Y}_k$ is the belonging vector shown in (4), being X the number of receivers in the barrier.

$$\mathbf{Y}_k = \begin{bmatrix} y_k^{(1,1} & \cdots & y_k^{(1,x} & \cdots & y_k^{(1,X} \\ y_k^{(2,1} & \cdots & y_k^{(2,x} & \cdots & y_k^{(2,X} \\ y_k^{(3,1} & \cdots & y_k^{(3,x} & \cdots & y_k^{(3,X} \\ y_k^{(4,1} & \cdots & y_k^{(4,x} & \cdots & y_k^{(4,X} \\ y_k^{(5,1} & \cdots & y_k^{(5,x} & \cdots & y_k^{(5,X} \end{bmatrix}_{5 \times X} \tag{5}$$

To evaluate if an established link j in the receiver x is not interrupted, the correlation value $y_k^{(j,x}$ should be higher than a determined detection threshold (T_H). But when the tracks are free of obstacles, the correlation value could be lower than the threshold due to the channel degradation (as was previously described), and consequently false alarms would be produced. To reduce false alarms, it was proposed in (Garcia et al., 2005) the use of a dynamic threshold, $T_{H,k}^{(j,x}$. This threshold is based on an H_∞ filter (Simon, 2000), and it is dynamically adapted considering meteorology and solar interference. The H_∞ filter gives an estimate $\hat{y}_k^{(j,x}$ of the correlation value $y_k^{(j,x}$ for every link j in every receiver x at every time instant, establishing the threshold in time instant k. But to avoid false alarms, it is necessary

to set a minimum threshold $T_{H\text{-}min}$, depending of the codification scheme and the expected noise. Equation (6) shows how the dynamic threshold is generated. Finally, for every link is generated an output $z_k^{(j,x)}$ corresponding to its state: *on* or *off*, as shown in (7). Similarly as (5), one matrix $\mathbf{Z}_k$ is obtained representing the state of all the links (1, on; 0, off). Figure 7 depicts the diagram block of a receiver tuned to a generic code considering the described process.
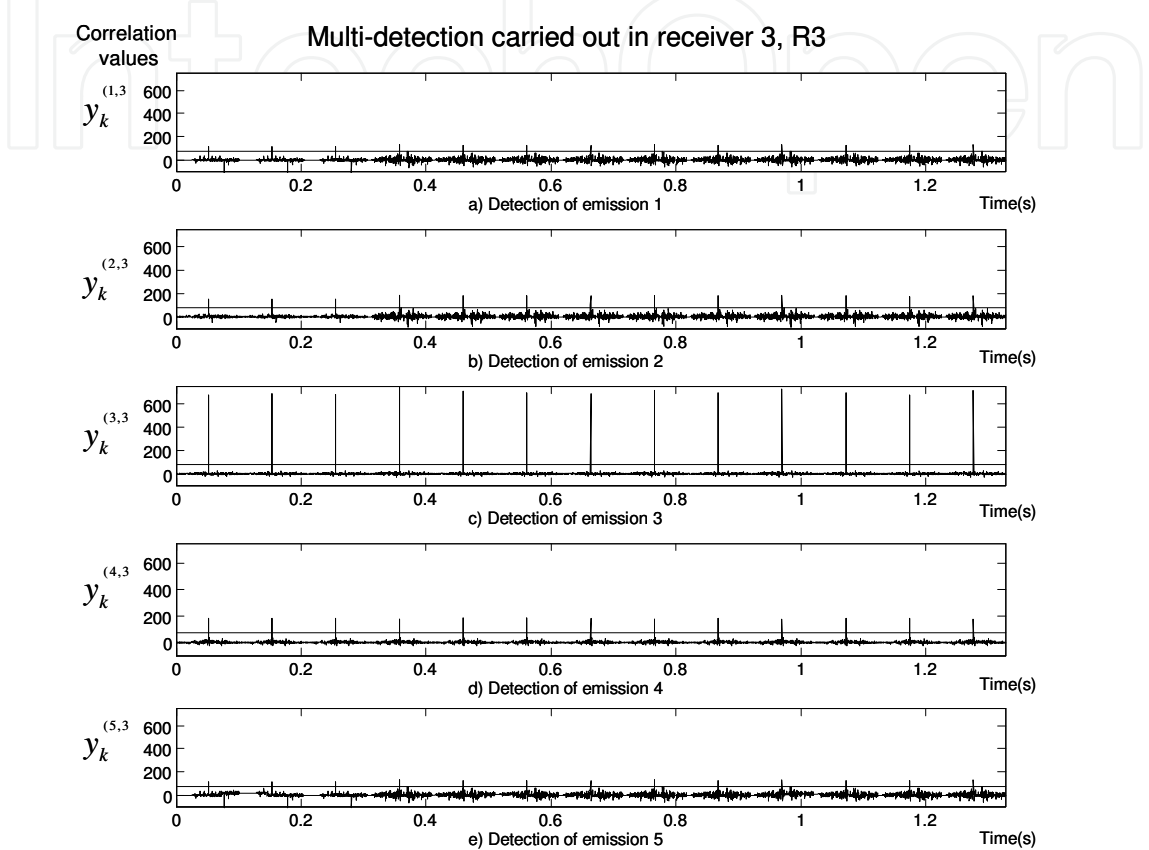

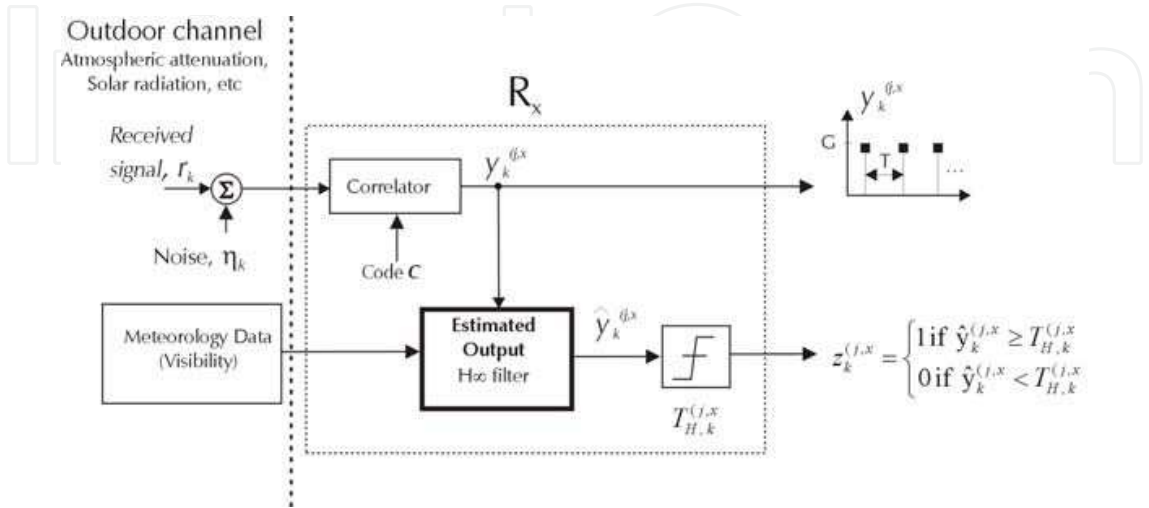Fig. 6. Real correlation outputs obtained in an IR receiver when the links are not interrupted.

Fig. 7. Block diagram of a receiver Rx tuned to a generic code C.

$$T_{H,k}^{(j,x)} = \max\left(\frac{\hat{y}_{k-1}^{(j,x)}}{2}, T_{H-\min} \right) \tag{6}$$

$$z_k^{(j,x)} = \begin{cases} 1 \text{ if } \hat{y}_k^{(j,x)} \geq T_{H,k}^{(j,x)} \\ 0 \text{ if } \hat{y}_k^{(j,x)} < T_{H,k}^{(j,x)} \end{cases} \tag{7}$$

As it is concluded from (6), threshold in time instant *k* depends on the estimated correlation output in time instant *k-1*, and the threshold will be adapted to the slow changes of the channel produced by weather conditions or solar radiation. On the contrary, if there exists an obstacle it will generate a fast change of the channel, causing a lack of signal in the receiver, and consequently, a low correlation value. As it is shown in (Garcia et al., 2005), this strategy reduces false alarms due to the channel degradation.

5. Sensor data fusion

In a railway environment, typical situations that can generate a false alarm must be identified. Although, the occurrence of false alarms has been notably reduced by using dynamic threshold in the detection stage, it is still possible for some receivers not to detect the emissions because a small object (moving leaves, small animals, etc.) has temporarily interrupted the link, or because weather conditions are severe, or, simply, because the corresponding emitter is damaged. These situations should not cause alarm activations for the existence of objects.

In detection, two pieces of information must be present in every sensor output (Klein, 2004). Firstly, the detection itself; the barriers provides this information in matrices $\mathbf{Y_k}$ and $\mathbf{Z_k}$. Secondly, how well, or with what confidence the sensor has been able to detect an object. For the latter, it is necessary to combine data from different sources, taking into account external variables such as weather conditions or sensor degradation. For the IR barrier, weather conditions can be modeled by considering *visibility*, as has been previously explained. There is a direct relation between visibility and atmospheric attenuation. It is also worth noting that the failure of just one individual link may be considered insignificant, since if a dangerous object exists, at least 10 links will be interrupted, as was described in Section 2.

Considering the above remarks, the data fusion has been carried out at two levels. Firstly, the detection area has been divided into 25cm-wide influence areas according to the receivers, so if a dangerous object exists, it is detected in two consecutive influence areas. The result of this level is a measurement of the certainty of existence of objects in every influence area. Secondly, values for the certainty of the existence of objects belonging to two consecutive influence areas have been fused by means of Dempster-Shafer evidential theory (Klein, 2004) to obtain a final value for the certainty of existence of objects larger than 50x50x50cm. Figure 8 shows a block diagram of the validation of obstacle detection considering the information that provides the barrier.

5.1 Certainty of existence of objects in the influence area, $A_{(x)}$

Figure 9 shows the division of the detection area into influence areas. The influence area of the receiver R_x is represented by $A_{(x)}$. After the analysis of the influence area, a value for the certainty of existence of objects is obtained represented by $c_{A(x)} \in [0, 1]$.
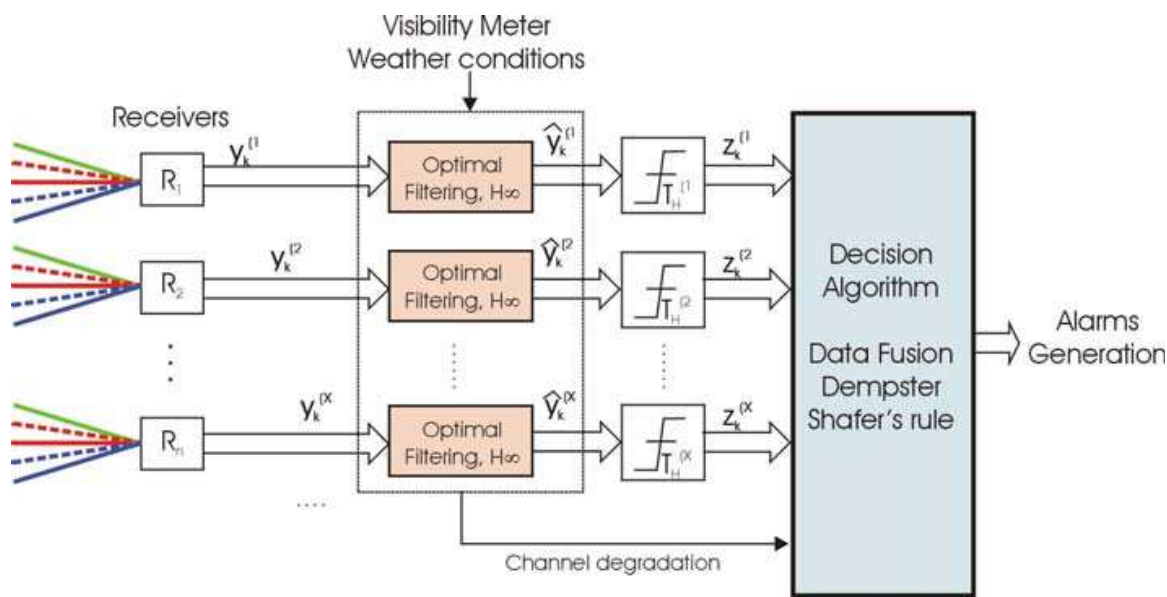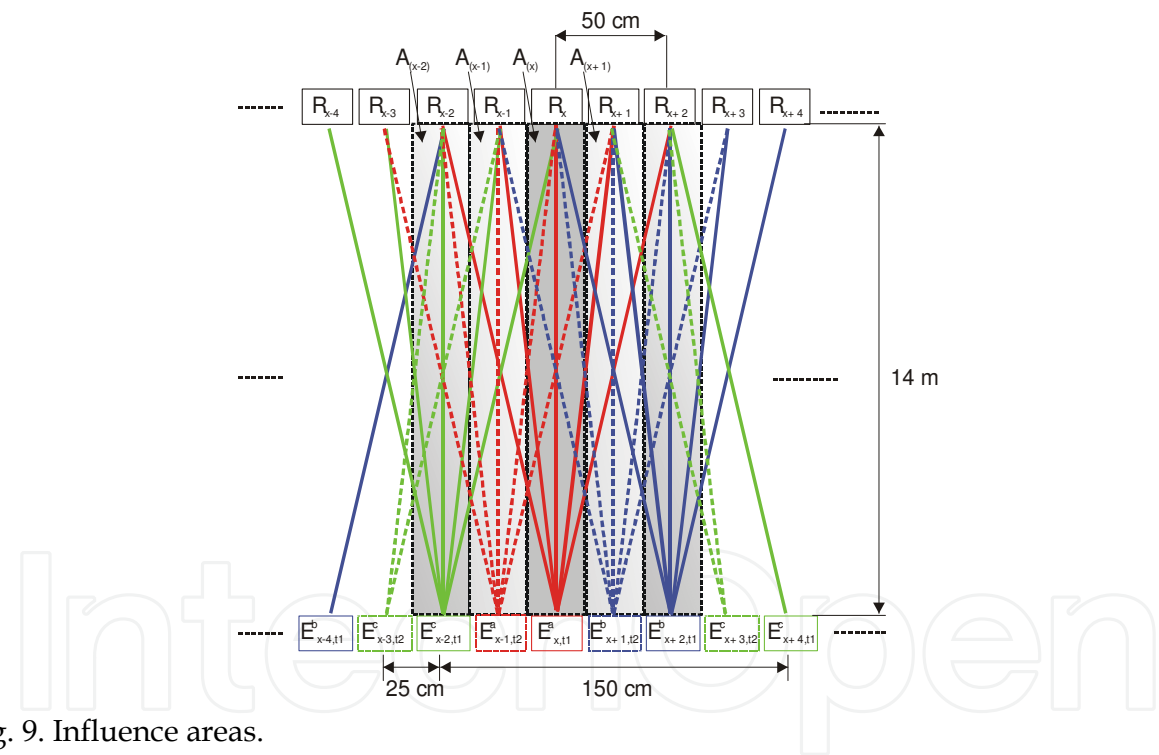
Fig. 8. Validation of obstacle detection.

Fig. 9. Influence areas.

As Figure 9 shows, and more detailed in Figure 10, there exist eleven links for every influence area, established between five emitters and five receivers. These links cross several areas, except for the link between the emitter x and the receiver x, that only exists in the area $A_{(x)}$.

To determine if a link is interrupted, it is only necessary to evaluate the state (*on*, *off*) of the corresponding element in the matrix $\mathbf{Z}_k$. Due to the fact that the channel degradation can generate a lack of signal in the detector, this situation can be mistaken for the existence of an object. For this reason, if at any k instant, $z_k^{(j,x}$ was zero –existence of an obstacle-, but a high-level channel degradation occurred at the $k\text{-}1$ instant, it would be very unlikely that the lack

of signal was produced by an object. Therefore, to obtain the certainty of the link interrupted by an object, the link degradation has to be considered.
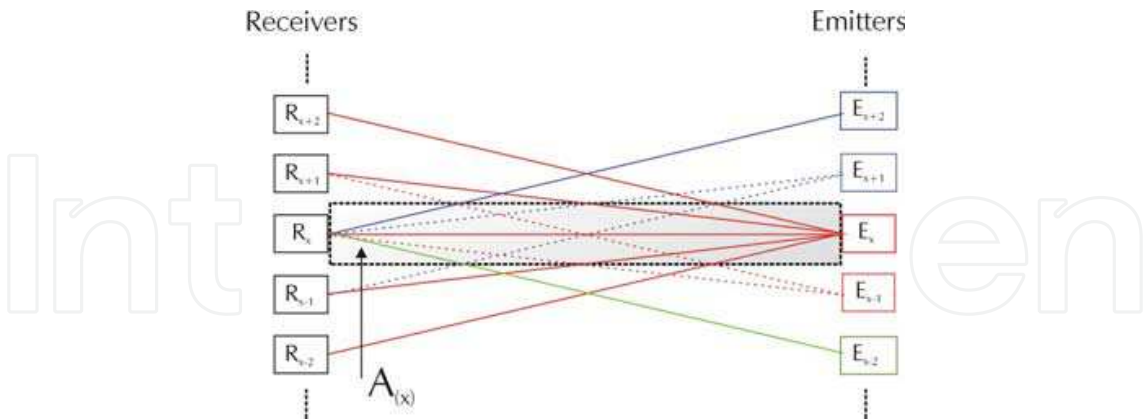

Fig. 10. Links for influence area $A_{(x)}$.

Furthermore, the probability of an object interrupting a link in the area $A_{(x)}$ depends on the percentage of the range of the link placed in such area. For the link between emitter x and receiver x (link $l_{x,x}$) the probability is one, but for the rest is 0.5 or 0.25. Table 2 shows the probability $\rho_{e,r}$ for every link inside a detection area. Sub-indexes e and r denote the x position of the emitter and the receiver respectively.

Index i	-5	-4	-3	-2	-1	0	1	2	3	4	5
Link $l_{e,r}$	$l_{x,x-2}$	$l_{x,x-1}$	$l_{x+1,x-1}$	$l_{x-2,x}$	$l_{x-1,x}$	$l_{x,x}$	$l_{x+1,x}$	$l_{x+2,x}$	$l_{x-1,x+1}$	$l_{x,x+1}$	$l_{x,x+2}$
Probability $\rho_{e,r}$	0.25	0.5	0.5	0.25	0.5	1	0.5	0.25	0.5	0.5	0.25

Table 2. Probability of an object interrupting a link in the area $A_{(x)}$.

Regarding this, the certainty of interruption of a link by an object between the emitter e and the receiver r is the following:

$$\sigma_{e,r} = \alpha_{e,r} \cdot \rho_{e,r} \qquad (8)$$

where $\alpha_{e,r}$ is the channel degradation before the interruption of the link; and $\rho_{e,r}$ is the probability of the object to be in the area $A_{(x)}$. The value of $\alpha_{e,r}$ is empirically computed according to Figure 11.
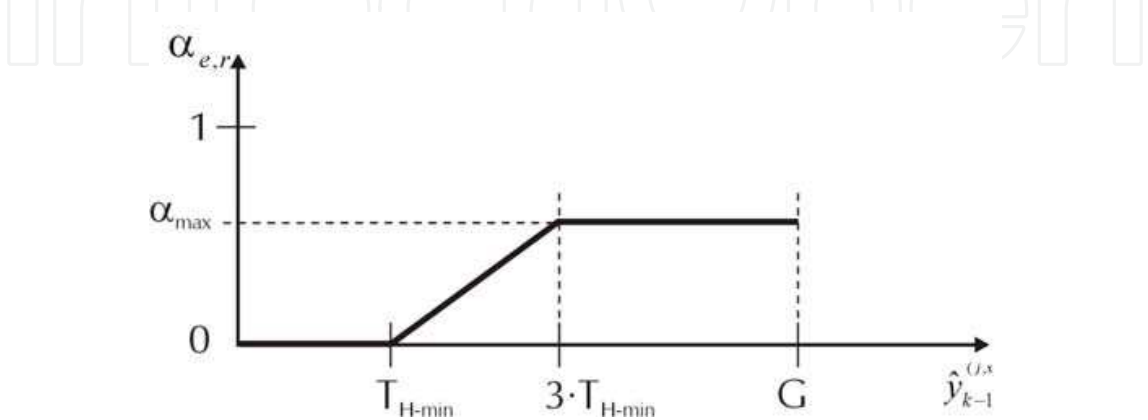

Fig. 11. Calculation of $\alpha_{e,r}$.

In Figure 11, $\alpha_{max}=0.5$; $T_{H\text{-}min}$ is the minimum threshold; G is the process gain -see (3)-; and $\hat{y}_{k-1}^{(j,x)}$ is the estimate of the correlation carried out by the H_∞ filter at $k\text{-}1$ instant (before the interruption of the link). This estimate can be considered as a channel degradation measurement, and it corresponds to the link between the emitter e and the receiver r. After obtaining $\sigma_{e,r}$, the value for the certainty of the existence of obstacles in the area $A_{(x)}$ is computed considering the eleven links. If it is assumed that the probability of the link $l_{e,r}$ being interrupted by an object is $\sigma_{e,r}$, then $c_{A(x)}$ is obtained as the union probability of independent events, as (9) shows. In (9), for convenience, the probability of every link is represented by $P(l_i)$ ($P(l_i)=\sigma_{e,r}$), and i represents every link according to the assignment done in Table 2.

$$
\begin{aligned}
&P(l) = 0; \\
&for\ i = \text{-}5; i \leq 5; i++ \\
&\qquad P(l_i \cup l) = P(l_i) + P(l) - P(l_i) \cdot P(l) \\
&\qquad P(l) = P(l_i \cup l) \\
&endfor \\
&c_{A(x)} = P(l)
\end{aligned}
\tag{9}
$$

It is important to remark that if the number of interrupted links in a barrier provides a value for the corresponding $c_{A(x)}>0.5$, then it is very possible than an object exists in the area $A_{(x)}$, but it can not be concluded if it is larger than minimum dimensions.

5.2 Dempster-Shafer's theory application

Once the values for the certainty of existence of objects are available for every area, they can be combined between consecutive areas $A_{(x)}$ and $A_{(x+1)}$, in order to obtain the certainty of existence of objects larger than 50x50x50cm. According to the Dempster-Shafer's theory (Klein, 2004), if $c_{A(x)}$ is considered as the probability mass of the certainty of existence of objects in the area $A_{(x)}$, a value $c_{o,x} \in [0,1]$ can be obtained as shows (10), representing the result of the fusion between the areas $A_{(x)}$ and $A_{(x+1)}$.

$$
c_{o,x} = \frac{c_{A(x)} \cdot c_{A(x+1)}}{1 - \left(1 - c_{A(x)}\right) \cdot c_{A(x+1)} - \left(1 - c_{A(x+1)}\right) \cdot c_{A(x)}}
\tag{10}
$$

The higher the value of $c_{o,x}$ is, the higher the certainty of existence of object larger than 50x50x50cm is. But if $c_{o,x}$ takes a value of 0.5, it means that there is a situation of uncertainty (it can not be concluded if there exists a dangerous object). Values of $c_{o,x}$ lower than 0.5 mean there is a certainty of absence of object.

All the components $c_{o,x}$ can be arranged in a vector $\mathbf{C_O}$ as (11) shows, being N_Z the number of influence areas. According to the number of consecutive components of vector $\mathbf{C_O}$ higher than 0.5, can be concluded how large the object is.

$$
\mathbf{C_O} = \begin{bmatrix} c_{o,1} & \cdots & c_{o,x} & \cdots & c_{o,(N_Z-1)} \end{bmatrix}
\tag{11}
$$

6. Real results

To evaluate the feasibility of the proposed data fusion algorithms, a prototype of the barrier has been used. Figure 12 shows an IR barrier prototype based on 4 emitters and 8 receivers. Figure 13 shows the established links among emitters and receivers and the detection areas. Notice that any area have eleven links as was explained, due to the fact that it is necessary 5 emitters, and in this situation only 4 have been used. This prototype carries out the encoding and detection schemes that have been previously described.

(a)   (b)

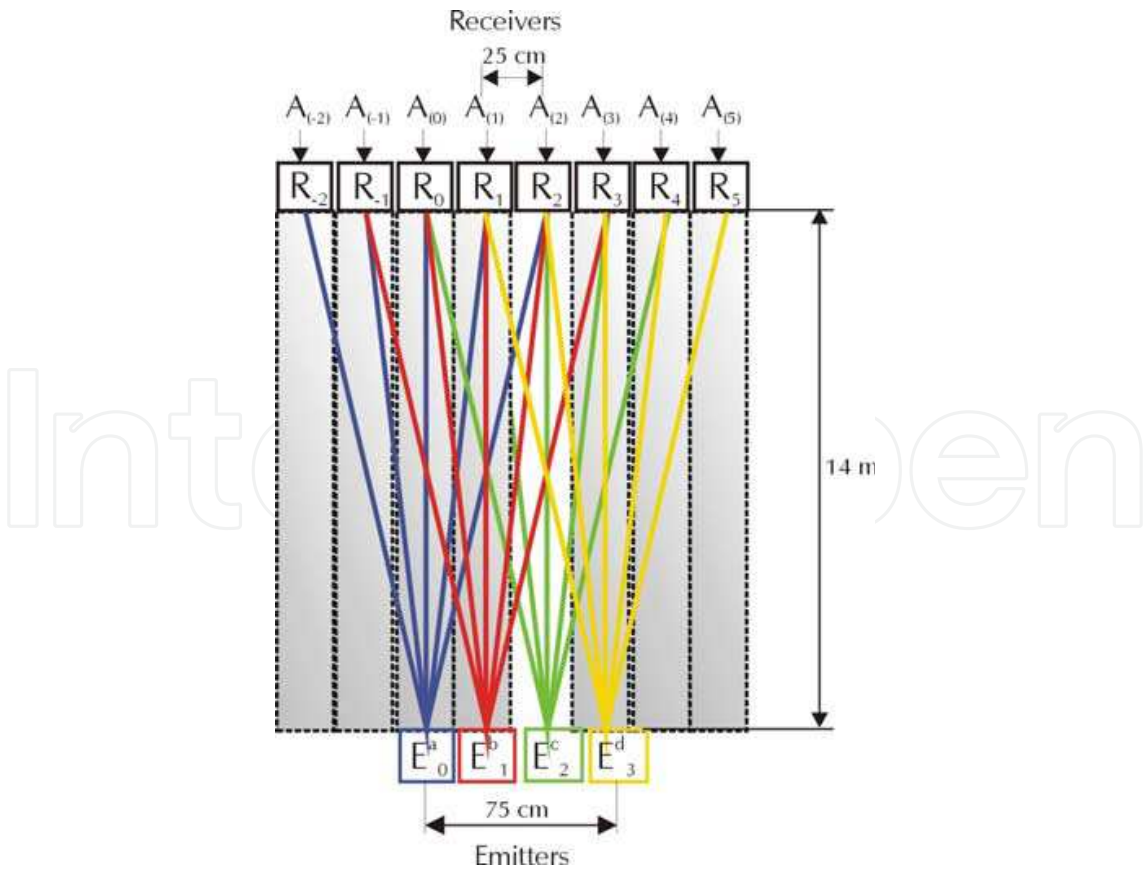Fig. 12. IR barrier prototype: (a) Emitter barrier; (b) Receiver barrier.

Fig. 13. Established links and detection areas using the prototype of the barrier.

Focusing on the data fusion algorithms, two situations have been tested: firstly, when an object larger than 50 cm of side is between the barriers; and secondly, when there exist random cuts of the links.

Figure 14 shows the scheme of a real example of detection, when one dangerous object (larger than 50x50x50cm) is inside the detection area. Table 3 shows all the relevant information that it is necessary for applying the algorithm belonging to $A_{(1)}$ and $A_{(2)}$ (the rest of areas have been omitted for simplicity): first column shows the established links in each area; second column, the estimate of the correlation values carried out by the H_∞ filter in k-1 instant for each link, $\hat{\mathbf{y}}_{k-1}^{(j,x)}$, when any link was interrupted; next columns show the channel degradation ($\alpha_{e,r}$) before the interruption of the link and the probability $\rho_{e,r}$ of the object to be in the area $A_{(x)}$; and finally, last column shows the certainty of interruption of a link by an object, $\sigma_{e,r}$. In this test, $\alpha_{e,r}$ has been obtained as was shown in Figure 11. The minimum threshold $T_{H\text{-}min}$ is fixed to 50, α_{max} =0.5 and the process gain G is *1024*.
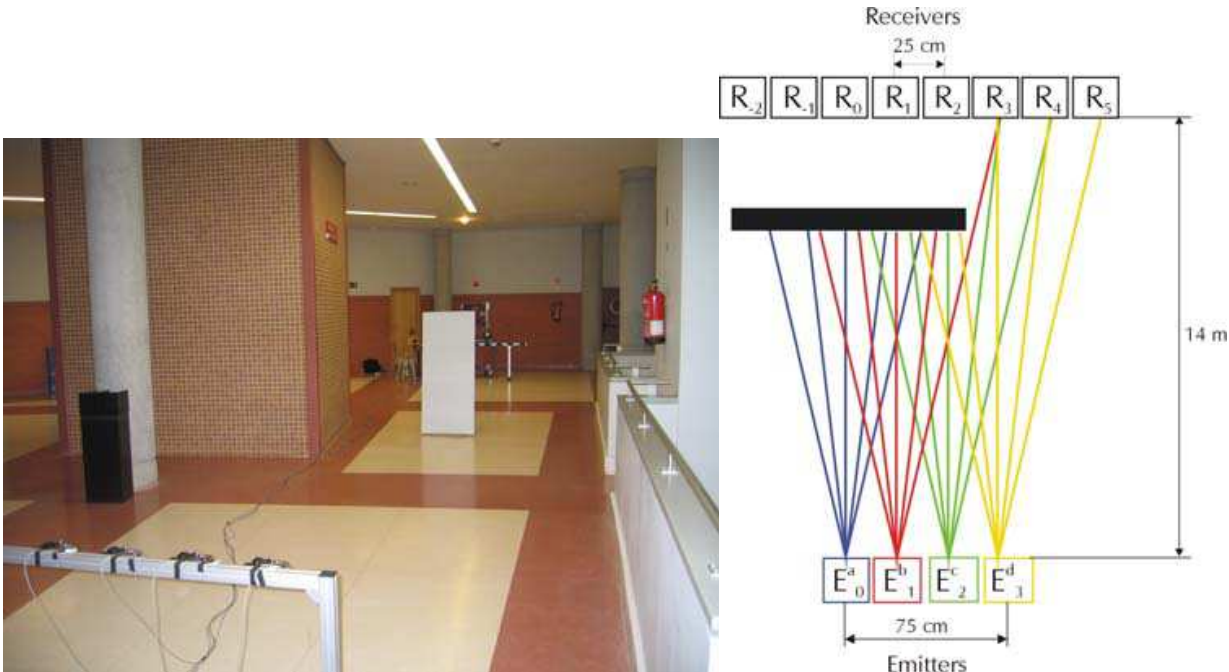

Fig. 14. Interrupted links when an object larger than 50 cm of side exists.

Then, the certainties of existence of objects in areas ($c_{A(x)}$) have been computed using the algorithm described (8)-(9). Finally, consecutive areas have been combined by using (10) to obtain the vector $\mathbf{C_o}$, containing the certainty of existence of objects larger than 50x50x50cm. Table 4 shows the interrupted links (e,r), and the obtained results for $c_{A(x)}$ and the vector $\mathbf{C_o}$.

As the results show there is a high certainty (higher than 0.7) of the existence of an object larger than 50x50x50cm, between areas $A_{(-1)}$ y $A_{(0)}$, $A_{(0)}$ and $A_{(1)}$, and $A_{(1)}$ y $A_{(2)}$. Due to the fact that these areas are consecutive ones, it could be concluded that the size of the object (x dimension) is between 75 and 100 cm.

Figure 15 displays a different situation. In this case, there are random cuts of the links, due to the existence of small objects. In a real situation it can be due to small animals, flying leaves, a sensor failure, etc. The applied method is the same that has been described in the

previous example. Table 5 shows the data fusion results, showing clearly a low certainty of the existence of dangerous objects (larger than 50x50x50 cm).

Area $A_{(1)}$				
Link (e,r)	$\hat{y}_{k-1}$	$\alpha_{e,r}$	$\rho_{e,r}$	$\sigma_{e,r}$
1,-1	60	0.05	0.25	0.012
1,0	207.2	0.5	0.5	0.25
2,0	102.8	0.26	0.5	0.13
0,1	145.1	0.47	0.5	0.23
1,1	416.8	0.5	1	0.5
2,1	99.3	0.24	0.5	0.12
3,1	55	0.02	0.25	0.005
0,2	66.7	0.08	0.5	0.04
1,2	252.5	0.5	0.5	0.25
1,3	73	0.11	0.25	0.027
Area $A_{(2)}$				
Link (e,r)	$\hat{y}_{k-1}$	$\alpha_{e,r}$	$\rho_{e,r}$	$\sigma_{e,r}$
2,0	102.8	0.26	0.25	0.065
2,1	99.3	0.24	0.5	0.12
3,1	55	0.02	0.5	0.01
0,2	66.7	0.08	0.25	0.02
1,2	252.5	0.5	0.5	0.25
2,2	321.3	0.5	1	0.5
3,2	130.3	0.4	0.5	0.2
1,3	73	0.11	0.5	0.055
2,3	345.1	0.5	0.5	0.25
2,4	203.2	0.5	0.25	0.125

Table 3. Real data belonging to detection areas $A_{(1)}$ and $A_{(2)}$ for the situation shown in Figure 14.

Interrupted links (*e,r*): (0,-2);(0,-1);(1,-1);(0,0);(1,0);(2,0);(0,1);(1,1);(2,1);(3,1); (0,2); (1,2); (2,2); (3,2)							
$A_{(-2)}$	$A_{(-1)}$	$A_{(0)}$	$A_{(1)}$	$A_{(2)}$	$A_{(3)}$	$A_{(4)}$	$A_{(5)}$
$C_{A(-2)}=0.125$	$C_{A(-1)}=0.44$	$C_{A(0)}=0.8$	$C_{A(1)}=0.84$	$C_{A(2)}=0.76$	$C_{A(3)}=0.2$	$C_{A(4)}=0$	$C_{A(5)}=0$
$c_{o,-2}=0.1$							
	$c_{o,-1}=0.75$						
		$c_{o,0}=0.95$					
			$c_{o,1}=0.94$				
				$c_{o,2}=0.44$			
					$c_{o,3}=0$		
						$c_{o,4}=0$	

$$\mathbf{C_O} = \begin{bmatrix} 0.1 & 0.75 & 0.95 & 0.94 & 0.44 & 0 & 0 \end{bmatrix}$$

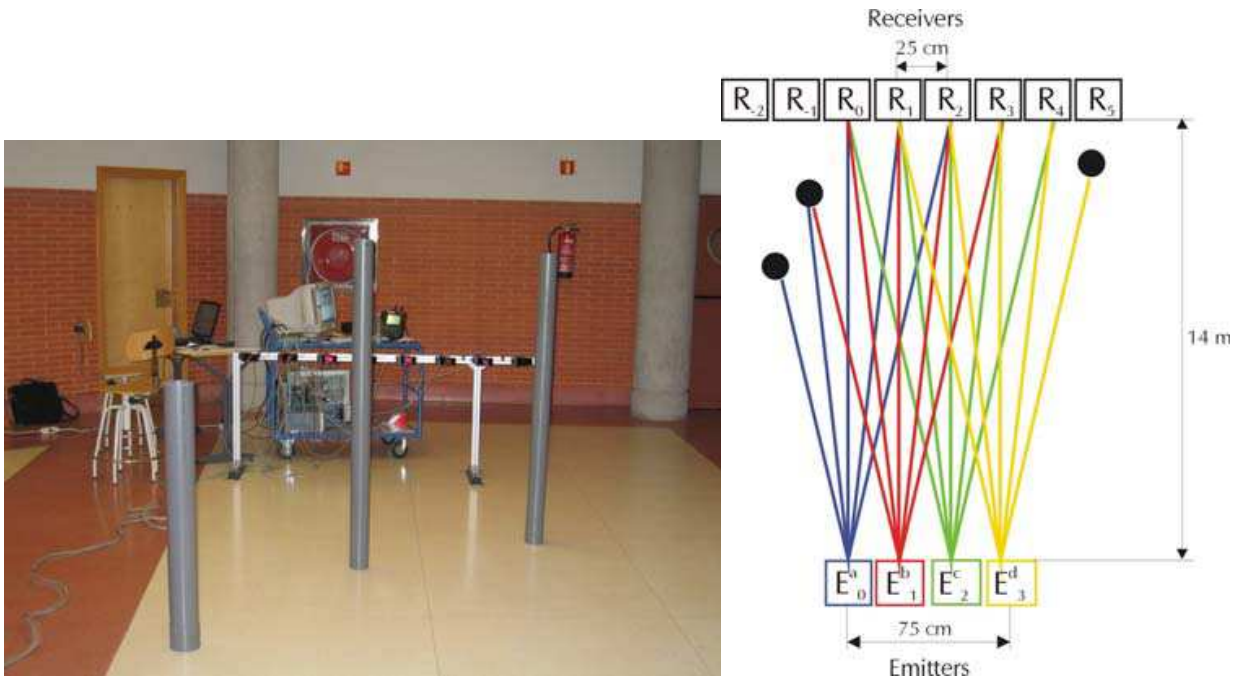Table 4. Data fusion results for the test shown in Figure 14.

Fig. 15. Interrupted links when there are random cuts of the links.

Interrupted links (*e,r*): (0,-2);(0,-1);(1,-1);(3,5)							
A$_{(-2)}$	**A$_{(-1)}$**	**A$_{(0)}$**	**A$_{(1)}$**	**A$_{(2)}$**	**A$_{(3)}$**	**A$_{(4)}$**	**A$_{(5)}$**
C$_{A(-2)}$=0.125	C$_{A(-1)}$=0.5	C$_{A(0)}$=0.25	C$_{A(1)}$=0	C$_{A(2)}$=0	C$_{A(3)}$=0.125	C$_{A(4)}$=0.25	C$_{A(5)}$=0.125

$c_{o,-2}$=0.125

$c_{o,-1}$=0.25

$c_{o,0}$=0

$c_{o,1}$=0

$c_{o,2}$=0

$c_{o,3}$=0.04

$c_{o,4}$=0.04

$$\mathbf{C_O} = \begin{bmatrix} 0.125 & 0.25 & 0 & 0 & 0 & 0.04 & 0.04 \end{bmatrix}$$

Table 5. Data fusion results for the test shown in Figure 15.

7. Conclusion

In this chapter, a real prototype of an infrared barrier for obstacle detection on the tracks has been presented. Due to the fact that detection is based on the lack of radiation in the receivers, the channel degradation can be mistaken with the existence of obstacles. For this reason, validation algorithms are necessary, in order to increase the reliability of the detection.

Sensor data fusion based on the evidential theory has been applied in order to obtain the certainty of the existence of dangerous obstacles for the railway traffic. The proposed fusion algorithm takes into account the spatial diversity of the links that are established in the barrier and how the channel degradation affects them. Real tests have been carried out, in order to validate the described algorithms, showing them successful results.

To improve the safety level required in this application, it is necessary to incorporate new sensory systems, as can be cameras or ultrasounds to make up for the infrared deficiencies. All the information provided by these new sensory systems, have to be fused with the IR barrier, in order to obtain reliable information about the existence of objects on the tracks that can suppose a risk for railway traffic.

8. Acknowledgments

9. References

Bloom, Scott; Korevaar, Eric; Schuster, John; Willebrand, Heinz. "Understanding the performance of free-space optics [Invited]". *Journal of Optical Networking*, June 2003, Vol 2 nº 6, pp 178-200

Chow, A. "Performance of spreading Codes for direct sequence code division multiple access (DS-CDMA)", Technical Report, 5 December 2003, Stanford University.

De Marziani, Carlos; Ureña, Jesús; Hernández, Álvaro; Mazo, Manuel; Álvarez, Fernando J. ; García, Juan Jesús; Donato, Patricio. "Modular Architecture for Efficient Generation and Correlation of Complementary Set of Sequences", *IEEE Transactions on Signal Processing*, Vol. 55, No. 5, May 2007, pp. 2323-2337

Díaz, M. J. ; García, J. Jesús; Hernández, Álvaro; Losada, Cristina; García, Enrique. "Advanced Multisensorial Barrier for Obstacle Detection". *Proceedings of IEEE International Symposium on Intelligent Signal Processing. WISP 2007*, Alcalá de Henares, Madrid, Spain, pp. 549-554

García, J. Jesús ; Losada, Cristina ; Espinosa, Felipe ; Ureña, Jesús ; Hernández, Álvaro Hernández ; Mazo, Manuel ; De Marziani, Carlos ; Jiménez, Ana ; Álvarez Fernando ; Jiménez, José A. "Optimal estimation techniques to reduce false alarms in railway obstacle detection". *Proceedings of IEEE International Conference on Industrial Technology. ICIT 2005*, Hong-Kong, China, pp 459-464

García, J. J., Ureña, J., Hernández, Á., Mazo, M., García, J.C., Álvarez, F., Jiménez, J. A., Donato, P., Pérez, C. "IR sensor array configuration and signal processing for detecting obstacles in railways" *Proceedigns Third IEEE Sensor Array and Multichannel Signal Processing Workshop* SAM 2004.

GIF, 2001. Gestor de Infraestructuras Ferroviarias. "System for falling obstacle detection on railway. Technical and functional requirements". (Published in Spanish). 2001.

GIF, 2004. Gestor de Infraestructuras Ferroviarias. "Functional description of the object fall detector based on infrared sensors. (Published in Spanish). 2004

Kim, Isaac I. ; Stieger, Ron ; Koontz, Joseph A.; Moursund, Carter; Barclay, Micah ; Adhikari, Prasanna ; Schuster, John ; Korevaar, Eric; Ruigrok, Richard; DeCusatis, Casimer. "Wireless optical transmission of fast ethernet, FDDI, ATM, and ESCON protocol data using the TerraLink laser communication system", *Optical Engineering*, Vol. 37 No. 12, December 1998

Kim, Isaac I.; McArthur, Bruce; Korevaar, Eric. "Comparison of laser beam propagation at 785 nm and 1550 nm in fog and haze for optical wireless communications", whitepapers, Optical Access, January 2000.

Klein, Lawrence A., "Data and sensor fusion: a tool for information assessment and decision making", *Spie Press*, 2004.

Simon, D. "From here to infinity ". *Embedded Systems Programming Magazine*. July, 2000. pp. 2-9

Tseng, Shu-Ming & Bell, M.R.; "Asynchronous multicarrier DS-CDMA using mutually orthogonal complementary sets of sequences", *IEEE Transactions on Communications*, Volume 48, Issue 1, Jan. 2000, pp 53 – 59.

Yokota, Tomoharu; Asaka, Kazuhiko; Matsumoto, Hideki; Yamaguchi, Tsuyoshi; Kasai, Chiharu. "A Study on Improving the Link Quality of the Free Space Optical Transmission System", Online. http://www.icsa.gr.jp/english/e_article_0103.htm, 2002.

Sensor and Data Fusion

Edited by Nada Milisavljevic

ISBN 978-3-902613-52-3

Hard cover, 436 pages

Publisher I-Tech Education and Publishing

Published online 01, February, 2009

Published in print edition February, 2009

Data fusion is a research area that is growing rapidly due to the fact that it provides means for combining pieces of information coming from different sources/sensors, resulting in ameliorated overall system performance (improved decision making, increased detection capabilities, diminished number of false alarms, improved reliability in various situations at hand) with respect to separate sensors/sources. Different data fusion methods have been developed in order to optimize the overall system output in a variety of applications for which data fusion might be useful: security (humanitarian, military), medical diagnosis, environmental monitoring, remote sensing, robotics, etc.

How to reference

In order to correctly reference this scholarly work, feel free to copy and paste the following:

J. Jesús García, Jesús Ureña, Manuel Mazo and Álvaro Hernández (2009). IR Barrier Data Integration for Obstacle Detection, Sensor and Data Fusion, Nada Milisavljevic (Ed.), ISBN: 978-3-902613-52-3, InTech, Available from:
http://www.intechopen.com/books/sensor_and_data_fusion/ir_barrier_data_integration_for_obstacle_detection

INTECH

open science | open minds